Missense Mutations in the Human Nanophthalmos Gene *TMEM98* Cause Retinal Defects in the Mouse

Sally H. Cross,[1] Lisa Mckie,[1] Margaret Keighren,[1] Katrine West,[1] Caroline Thaung,[2,3] Tracey Davey,[4] Dinesh C. Soares,[*,1] Luis Sanchez-Pulido,[1] and Ian J. Jackson[1]

[1]MRC Human Genetics Unit, MRC Institute of Genetics and Molecular Medicine, University of Edinburgh, Edinburgh, United Kingdom
[2]Moorfields Eye Hospital NHS Foundation Trust, London, United Kingdom
[3]University College London Institute of Ophthalmology, London, United Kingdom
[4]Electron Microscopy Research Services, Newcastle University, Newcastle, United Kingdom

Correspondence: Sally H. Cross, MRC Human Genetics Unit, MRC Institute of Genetics and Molecular Medicine, University of Edinburgh, Crewe Road, Edinburgh EH4 2XU, UK;
sally.cross@igmm.ed.ac.uk.

Current affiliation: *ACS International Ltd., Oxford, United Kingdom

Submitted: October 10, 2018
Accepted: May 28, 2019

Citation: Cross SH, Mckie L, Keighren M, et al. Missense mutations in the human nanophthalmos gene *TMEM98* cause retinal defects in the mouse. *Invest Ophthalmol Vis Sci*. 2019;60:2875–2887. https://doi.org/10.1167/iovs.18-25954

Purpose. We previously found a dominant mutation, *Rwbs*, causing white spots on the retina accompanied by retinal folds. Here we identify the mutant gene to be *Tmem98*. In humans, mutations in the orthologous gene cause nanophthalmos. We modeled these mutations in mice and characterized the mutant eye phenotypes of these and *Rwbs*.

Methods. The *Rwbs* mutation was identified to be a missense mutation in *Tmem98* by genetic mapping and sequencing. The human *TMEM98* nanophthalmos missense mutations were made in the mouse gene by CRISPR-Cas9. Eyes were examined by indirect ophthalmoscopy and the retinas imaged using a retinal camera. Electroretinography was used to study retinal function. Histology, immunohistochemistry, and electron microscopy techniques were used to study adult eyes.

Results. An I135T mutation of *Tmem98* causes the dominant *Rwbs* phenotype and is perinatally lethal when homozygous. Two dominant missense mutations of *TMEM98*, A193P and H196P, are associated with human nanophthalmos. In the mouse these mutations cause recessive retinal defects similar to the *Rwbs* phenotype, either alone or in combination with each other, but do not cause nanophthalmos. The retinal folds did not affect retinal function as assessed by electroretinography. Within the folds there was accumulation of disorganized outer segment material as demonstrated by immunohistochemistry and electron microscopy, and macrophages had infiltrated into these regions.

Conclusions. Mutations in the mouse orthologue of the human nanophthalmos gene *TMEM98* do not result in small eyes. Rather, there is localized disruption of the laminar structure of the photoreceptors.

Keywords: nanophthalmos, mouse models, retina, genetic diseases

There are a range of genetic disorders that present with a reduced eye size. In microphthalmia the reduced size is often associated with additional developmental eye defects, such as coloboma, and may also include developmental defects in other organs. In some cases there is an overall size reduction without other developmental defects. The smaller eye may be a result of a reduction in size of the anterior segment alone (anterior microphthalmos), the posterior segment alone (posterior microphthalmos), or a reduction of both. This last category includes simple microphthalmos and the more severe nanophthalmos.[1,2] Posterior microphthalmos is sometimes considered as part of a continuum with nanophthalmos, as they have pathological and genetic features in common. In nanophthalmos eye length is reduced by 30% or more, and is usually associated with other ocular features, notably a thickened choroid and sclera, as well as a high incidence of glaucoma, corneal defects, vascular defects, and a range of retinal features including retinitis pigmentosa, retinoschisis, retinal detachments, and retinal folds. Retinal folds are also observed in posterior microphthalmos, and are sometimes ascribed to a relative overgrowth of neural retina within a smaller globe, resulting in folding of the excess retinal tissue.

A number of genes have been found to be associated with nanophthalmos.[2] Mutations in three genes have established associations with nanophthalmos. Several families with nanophthalmos have been found to have clear loss-of-function mutations in both alleles of the gene encoding membrane-type frizzled related protein, *MFRP*, that is expressed principally in the retinal pigment epithelium (RPE) and ciliary body.[3] Homozygous loss-of-function mutations in *MFRP* have been found in other individuals with posterior microphthalmia plus retinitis pigmentosa, foveoschisis, and drusen, indicating likely genetic background effects on the severity or range of the disease.[4–6] A second autosomal recessive nanophthalmos gene is *PRSS56*, encoding a serine protease. Families with biallelic mutations in this gene have been characterized, some of whom have posterior microphthalmia while others have nanophthalmos.[7–9] There is no apparent genotype–phenotype correlation; there are patients with homozygous frameshift mutations with either condition. Intriguingly, association of variants at *PRSS56*

with myopia has been reported in genome-wide association studies.[10,11]

Most recently three families have been characterized in which heterozygous mutations in *TMEM98* are segregating with nanophthalmos. Two families have missense mutations; the third has a 34-bp (base pair) deletion that removes the last 28 bases of exon 4 and the first 6 bases of intron 4 including the splice donor site.[12,13] The effect of the deletion on the *TMEM98* transcript is unknown, but in silico splicing prediction programs (Alamut Visual Splicing Predictions) predict that it could result in exon 4 being skipped and the production of a potentially functional protein with an internal deletion. Alternatively, other splice defects would result in frameshifts, nonsense-mediated decay, and loss of protein from this allele. In this case the cause of the disease would be haploinsufficiency. Caution in assigning a role for *TMEM98* in nanophthalmos has been raised by findings in another study in which different heterozygous missense mutations in *TMEM98* were found in patients with high myopia and cone-rod dystrophy.[14]

Patients with heterozygous or homozygous mutations in the *BEST1* gene can have a range of defects.[15] *BEST1* encodes the bestrophin-1 protein, a transmembrane protein located in the basolateral membrane of the RPE.[16] The predominant disease resulting from heterozygous mutations in *BEST1* is Best vitelliform macular dystrophy, in which subretinal lipofuscin deposits precede vision defects.[17] These patients in early stages have a normal electroretinogram (ERG) but have a defect in electrooculography (EOG) indicative of an abnormality in the RPE. This can progress to retinitis pigmentosa. Five families have been reported with dominant vitreoretinochoroidopathy and nanophthalmos due to three different missense mutations in *BEST1*. Each mutant allele can produce two isoforms, one containing a missense mutation and one containing an in-frame deletion.[18] On the other hand, homozygous null mutations of *BEST1* result in high hyperopia accompanied by abnormal ERGs and EOGs and RPE abnormalities but lacking the vitelliform lesions found in the dominant disease.[19] Similar associations have been seen for mutations in the *CRB1* gene that encodes an apical transmembrane protein important for determining cell polarity in photoreceptors.[20] *CRB1* mutations are most frequently found associated with recessive retinitis pigmentosa or with Leber congenital amaurosis, and the disease phenotype observed in patients is very variable, suggestive of the influence of genetic modifiers.[21,22] In addition, hypermetropia and short axial length are common associations.[23] Furthermore, in two cases, both involving consanguineous families, the retinal dystrophy is associated with nanophthalmos.[24,25]

Mouse models with mutations in most of these genes have been analyzed. Mice that have targeted disruption of the *Best1* gene do not recapitulate the human bestrophinopathy phenotype or have only an enhanced response in EOG (indicative of a defect in the RPE).[26,27] However, when the common human mutation, W93C, is engineered into the mouse gene, both heterozygous and homozygous mice show a distinctive retinal pathology of fluid- or debris-filled retinal detachments that progress with age.[28] Spontaneous and targeted mutations in mouse *Crb1* have been characterized, and they showed similar, though not identical, recessive retinal phenotypes that had variable ages of onset.[29–31] The defects found are focal. Folds appear in the photoreceptor layer that are visualized as white patches on retinal imaging. In a complete loss-of-function allele and the frameshift allele $Crb1^{rd8}$, the folds are adjacent to discontinuities in the outer (external) limiting membrane (OLM) accompanied by loss of adherens junctions, and within them the photoreceptors, separated from the RPE, show degeneration.[29,30] In mice engineered to carry a missense mutation, $Crb1^{C249W}$, that causes retinitis pigmentosa in humans, although the OLM appears intact, retinal degeneration still occurs, albeit later than in the other models.[31] Similarly to the human phenotype, the extent of the retinal spotting observed in *Crb1* mutants is strongly affected by the genetic background.

Two lines of mice with spontaneous mutations in *Mfrp* have been described.[32–34] These do not recapitulate the nanophthalmic phenotype observed in humans. Instead, both have the same recessive phenotype of white spots on the retina, which correlate with abnormal cells below the retina that stain with macrophage markers, and progress to photoreceptor degeneration. For the $Mfrp^{rdx}$ mutation, atrophy of the RPE was reported,[33] and for $Mfrp^{rd6}$ a modest ocular axial length reduction from approximately 2.87 to 2.83 mm was reported although apparently not statistically significant.[35] A screen for mice with increased intraocular pressure (IOP) found a splice mutation in the *Prss56* gene predicted to produce a truncated protein.[8] The increased IOP was associated with a narrow or closed iridocorneal angle, analogous to that seen in human angle closure glaucoma. In addition these mice have eyes that are smaller than in littermates, although the size reduction is variable and slight, ranging from a 0% to 10% decrease in axial length. Reduction in axial length becomes statistically significant only after postnatal day 7. More recently it has been shown that mice deficient for *Prss56* have eyes with a decreased axial length and hyperopia.[36]

In summary, the human nanophthalmos mutations modeled in mice produce either a much less severe, or nonsignificant, axial length reduction (*Prss56*, *Mfrp*) or no effect on eye size (*Best1*, *Crb1*). There are differences in the development of human and mouse eyes, which probably underlies the differences in mutant phenotype.

To date no mouse models of *TMEM98* have been reported. We describe here characterization of a mouse mutation in *Tmem98*, which results in a dominant phenotype of retinal folds. In addition, we engineered the two human nanophthalmos-associated missense mutations of *TMEM98* into the mouse gene and show that these mice also, when homozygous or when compound heterozygous, have the same retinal fold phenotype but do not have a statistically significant reduction in eye size.

Materials and Methods

Mice

All mouse work was carried out in compliance with United Kingdom Home Office regulations under a United Kingdom Home Office project license, and experiments adhered to the ARVO Statement for the Use of Animals in Ophthalmic and Vision Research. Clinical examinations were performed as previously described.[37] Fundus imaging was carried out as described elsewhere.[38] Mice carrying a targeted knockout-first conditional-ready allele of *Tmem98*, $Tmem98^{tm1a(EUCOMM)Wtsi}$ (hereafter $Tmem98^{tm1a}$) were obtained from the Sanger Institute.[39] $Tmem98^{tm1a/+}$ mice were crossed with mice expressing Cre in the germline to convert this "knockout-first" allele to the reporter knockout allele $Tmem98^{tm1b(EUCOMM)Wtsi}$ (hereafter $Tmem98^{tm1b}$). In this allele the DNA between the loxP sites in the targeting cassette, which includes the neo-selection gene and the critical exon 4 of *Tmem98*, is deleted. To create the $Tmem98^{H196P}$ allele the CRISPR design site http://www.crispr.mit.edu (in the public domain) was used to design guides, and the selected guide oligos ex7_Guide1 and ex7_Guide2 (Supplementary Table S1) were annealed and cloned into the *Bbs I* site of the SpCas9 and chimeric guide

RNA expression plasmid px330[40] (pX330-U6-Chimeric_BB-CBh-hSpCas9 was a gift from Feng Zhang [Addgene plasmid #42230, https://www.addgene.org/; in the public domain]). Following pronuclear injection of this plasmid along with repair oligo H196P (Supplementary Table S1), the injected eggs were cultured overnight to the two-cell stage and transferred into pseudopregnant females. To create the *Tmem98*^{A193P} allele Edit-R crRNA (sequence 5′- CCAAUCACUGUCUGCCG CUG-3′) (Dharmacon, Lafayette, CO, USA) was annealed to tracrRNA (Sigma-Aldrich, St. Louis, MO, USA) in IDT Duplex buffer (IDT, Coralville, IA, USA). This, along with Geneart Platinum Cas9 nuclease (Invitrogen B25641; Carlsbad, CA, USA) and repair oligo A193P (Supplementary Table S1), was used for pronuclear injection as described above. Pups born were screened for the targeted changes by sequencing PCR fragments generated using the oligos ex7F and ex7R (Supplementary Table S2) and lines established carrying the targeted missense mutations. Genotyping was initially done by PCR, and sequencing where appropriate, using the primers in Supplementary Table S2. Subsequently most genotyping was performed by Transnetyx using custom designed assays (http://www.transnetyx.com, in the public domain). All lines were maintained on the C57BL/6J mouse strain background.

DNA Sequencing

The candidate interval was captured using a custom Nimblegen array and sequenced with 454 technology by Edinburgh Genomics (formerly known as GenePool) (http://www.genomics.ed.ac.uk, in the public domain).

Bioinformatics

Multiple protein sequence alignments were generated with the program Clustal Omega.[41] The possible impact of missense mutations on protein structure and function was evaluated using Polyphen-2 (http://genetics.bwh.harvard.edu/pph2/, in the public domain).[42] HMM-HMM comparison was used for protein homology detection.[43] For protein structure prediction Phyre2 was used (http://www.sbg.bio.ic.ac.uk/phyre2/, in the public domain).[44] We used PyMOL for protein structure visualization.[45] SCWRL[46] and the FoldX web server[47] were used to evaluate the effect of amino acid substitutions on protein stability.

Electroretinography

Prior to electroretinography, mice were dark adapted overnight (>16 hours), and experiments were carried out in a darkened room under red light using an HMsERG system (Ocuscience, Henderson, NV, USA). Mice were anesthetized using isofluorane and their pupils dilated by the topical application of 1% wt/vol tropicamide. Three grounding electrodes were placed subcutaneously (tail and each cheek), and silver-embedded electrodes were positioned on the corneas using hypromellose eye drops (2.5% methylcellulose coupling agent) held in place with a contact lens. Animals were kept on a heated platform to maintain them at 37°C and monitored using a rectal thermometer. A modified QuickRetCheck (Ocuscience) protocol was used for obtaining full-field scotopic ERGs. Briefly, four flashes at 10 mcd.s/m^2 at 2-second intervals were followed by four flashes at 3 cd.s/m^2 (at 10-second intervals) and then four flashes at 10 cd.s/m^2 (at 10-second intervals).

Histology and Immunostaining

Mice were culled and eyes enucleated and placed into Davidson's fixative (28.5% ethanol, 2.2% neutral buffered formalin, 11% glacial acetic acid) for 1 hour (cryosectioning) or overnight (wax embedding) except for the eye used for Figure 1, which was placed in 10% neutral buffered formalin for 24 hours before immersion in Davidson's fixative. Prior to wax embedding, eyes were dehydrated through an ethanol series. Hematoxylin and eosin staining was performed on 5- or 10-μm paraffin-embedded tissue sections and images captured using a Nanozoomer XR scanner (Hamamatsu, Hamamatsu City, Japan) and viewed using NDP.view2 software (Hamamatsu). For cryosectioning, fixed eyes were transferred to 5% sucrose in PBS and once sunk transferred to 20% sucrose in PBS overnight. Eyes were then embedded in optimum cutting temperature (OCT) compound and cryosectioned at 14 μM. For immunostaining on cryosections, slides were washed with water, then PBS, and postfixed in acetone at −20°C for 10 minutes. They were then rinsed with water, blocked in 10% donkey serum (DS), 0.1% Tween-20 in TBS (TBST) for 1 hour, and then incubated with primary antibodies diluted in TBST with 5% DS for 2 hours at room temperature or overnight at 4°C. Subsequently, after washing with TBST, the slides were incubated with Alexa Fluor secondary antibodies (Invitrogen) diluted 1:400 in TBST with 5% DS at room temperature for 1 hour. Following washing with TBST, coverslips were mounted on slides in Prolong Gold (ThermoFisher Scientific, Waltham, MA, USA) and confocal images acquired on a Nikon A1R microscope (Nikon, Tokyo, Japan). Images were processed using either NIS-Elements (Nikon) or ImageJ software (National Institutes of Health, Bethesda, MD, USA).

Eye Size Measurement

Eyes from male mice were enucleated and kept in PBS prior to measuring to prevent drying out. The analysis was restricted to males as significant differences in axial length have been reported in the C57BL/6J strain between male and female mice.[48] Axial length measurements were made from the base of the optic nerve to the center of the cornea using a Mitutoyo Digital ABS Caliper (6″/150 mm, #500-196-20; Kawasaki, Japan).

Antibodies

Primary antibodies used are listed in Table 1. DNA was stained with TOTO-3 (Invitrogen) or 4′,6-diamidine-2′-phenylindole dihydrochloride (DAPI).

Transmission Electron Microscopy

Samples were fixed in 2% electron microscopy grade glutaraldehyde (TAAB Laboratory Equipment, Aldermaston, UK) in sodium cacodylate buffer at 4°C overnight, postfixed in 1% osmium tetroxide (Agar Scientific, Essex, UK), dehydrated in increasing concentrations of acetone, and impregnated with increasing concentrations of epoxy resin (TAAB Laboratory Equipment). Embedding was carried out in 100% resin at 60°C for 24 hours. Semithin survey sections of 1 μm, stained with toluidine blue, were taken to determine relevant area. Ultrathin sections (approximately 70 nm) were then cut using a diamond knife on a Leica EM UC7 ultramicrotome (Leica, Allendale, NJ, USA). The sections were stretched with chloroform to eliminate compression and mounted on Pioloform-filmed copper grids (Gilder Grids, Grantham, UK). To increase contrast the grids were stained with 2% aqueous uranyl acetate and lead citrate (Leica). The grids were examined using a Philips CM 100 Compustage (FEI) Transmission Electron Microscope (Amsterdam, Netherlands). Digital images were collected using an AMT CCD camera (Deben UK Ltd., Suffolk, UK).

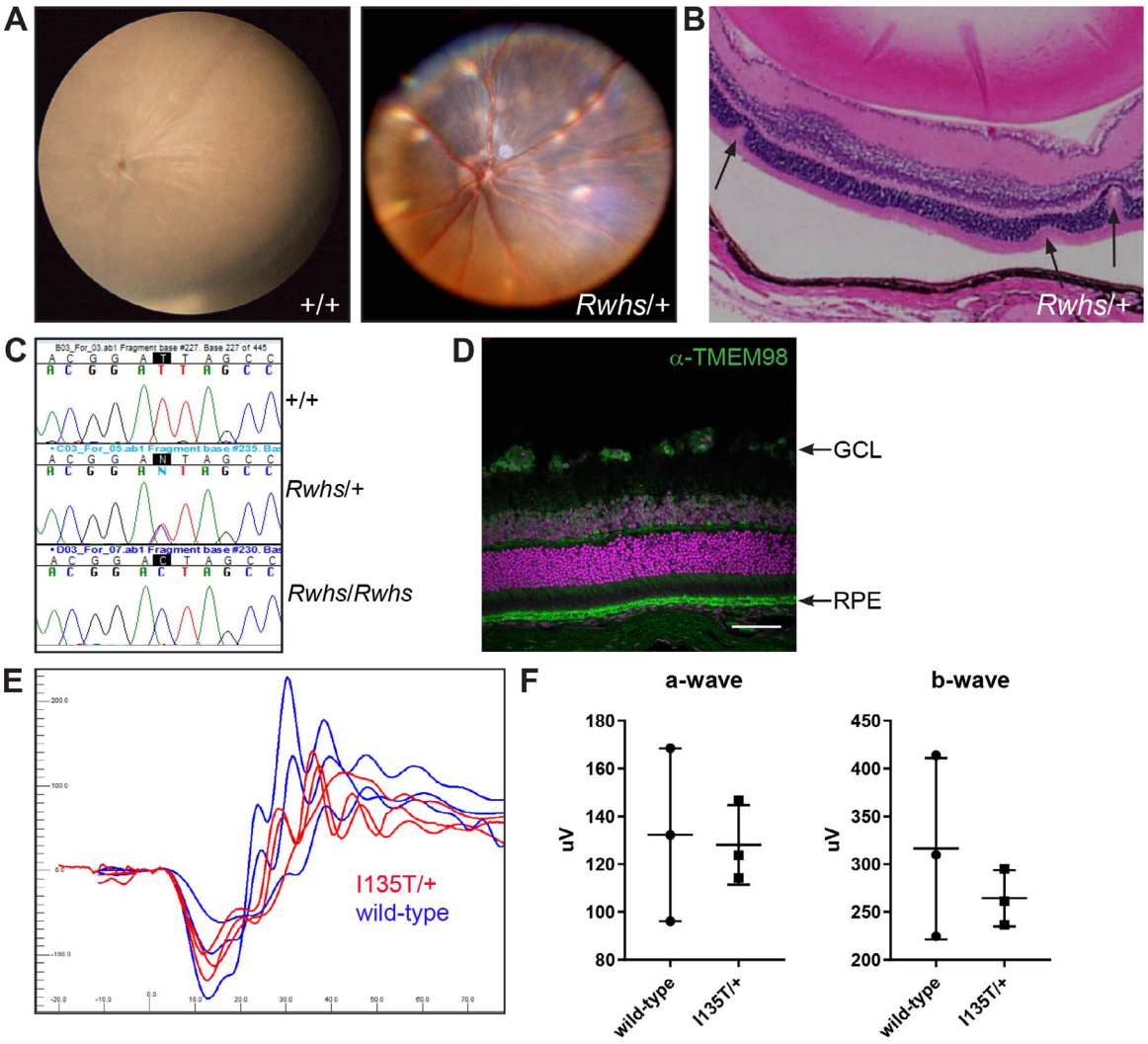

Figure 1. The *Rwhs* mutation is caused by an I135T mutation of the transmembrane gene *Tmem98*. (**A**) Retinal images of wild-type (+/+) and *Rwhs*/+ eyes. Scattered white spots are present on the *Rwhs*/+ retina. (**B**) *Rwhs*/+ retinal section with three folds in the outer nuclear layer indicated by *arrows*. The separation of the RPE from the outer segments is a fixation artifact. (**C**) Genomic DNA sequence traces from exon 5 of *Tmem98* from wild-type (+/+), heterozygous mutant (*Rwhs*/+), and homozygous mutant (*Rwhs*/*Rwhs*) embryonic samples. The position of the T-to-C transition at position 404 (404T>C) in the coding sequence of *Tmem98* is *highlighted*. (**D**) A section of wild-type retina immunostained for TMEM98 (*green*). Prominent staining is seen in the retinal pigment epithelium (RPE) and there is also some staining in the ganglion cell layer (GCL). DNA is shown in *magenta*. (**E**) $Tmem98^{I135T/+}$ mice have a normal ERG response. Shown are the responses at 3 cd.s/m^2 (average of four flashes) for the left eye of three $Tmem98^{I135T/+}$ mice (5–6 months of age) in *red* and three wild-type mice (5 months of age) in *blue*. (**F**) Comparison of a-wave amplitudes (*right*) and b-wave amplitudes (*left*), average of left and right eye for each mouse. There is no significant difference between $Tmem98^{I135T/+}$ and wild-type mice (a-wave, unpaired *t*-test with Welch's correction, $P = 0.87$ and b-wave, unpaired *t*-test with Welch's correction, $P = 0.45$). *Scale bar*: 100 μm (**D**).

Table 1. Primary Antibodies

Antibody	Source	Product No.	Concentration Used
anti-TMEM98	Proteintech (Rosemont, IL, USA)	14731-1-AP	1:5000, WB; 1:100, IF
anti-α-tubulin	Sigma-Aldrich	T5168	1:10,000, WB
anti-prominin 1	Proteintech	18470-1-AP	1:100, IF
anti-rhodopsin	Millipore (Burlington, MA, USA)	MAB5356	1:500, IF
anti-ML opsin	Millipore	AB5405	1:500, IF
anti-GFAP	Abcam (Cambridge, UK)	ab7260	1:500, IF
anti-β-catenin	Cell Signaling Technology (Danvers, MA, USA)	19807S	1:500, IF
anti-F4/80	Bio-rad (Hercules, CA, USA)	MCA497EL	1:500, IF

WB, Western blotting; IF, immunofluorescence.

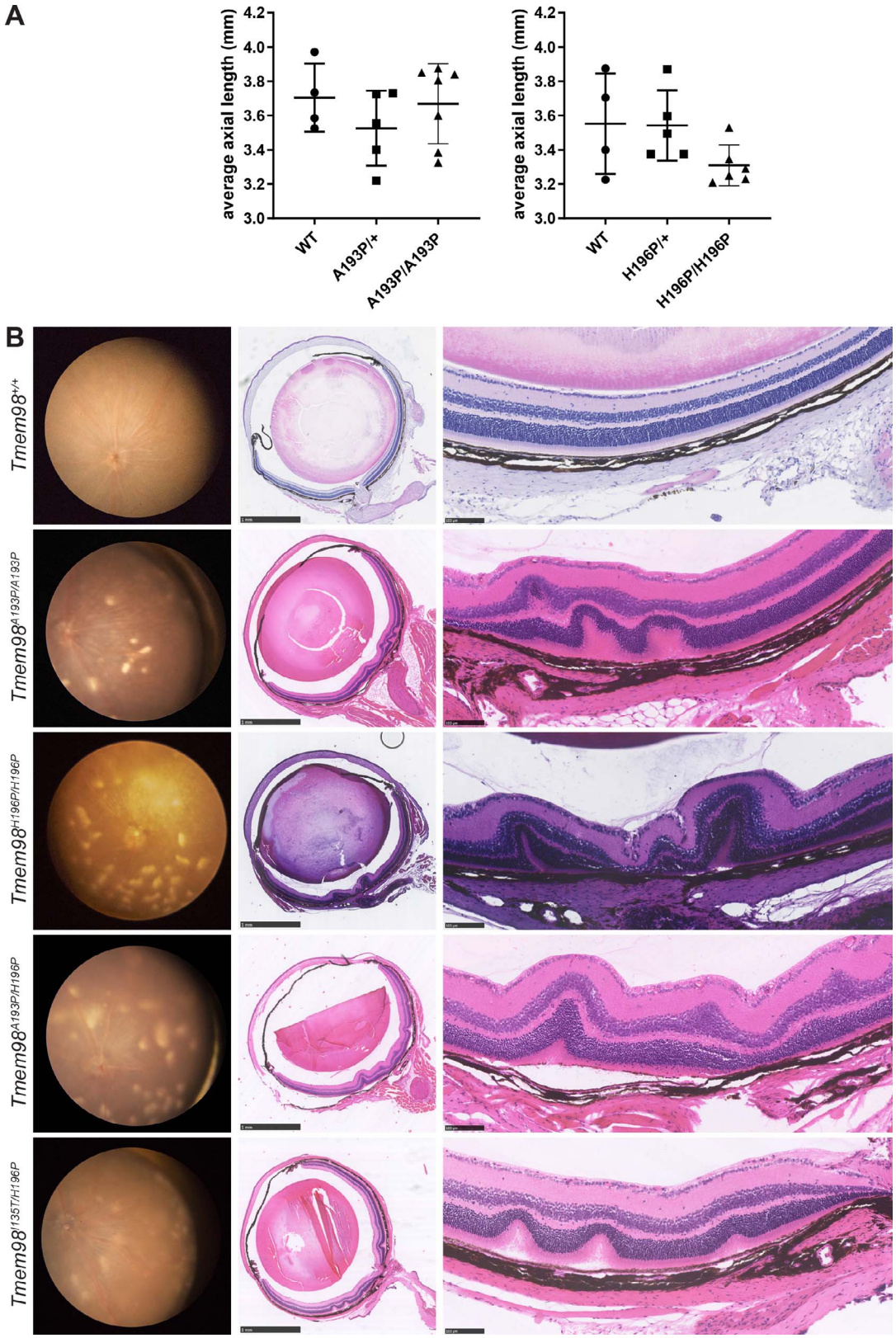

Figure 2. Eye phenotypes of homozygous and compound heterozygous mice with missense mutations of *Tmem98*. (**A**) Axial length measurements. Shown are the average axial length measurements for each mouse. (**B**) *Left*: retinal images; *center*: sections through the optic nerve; *right*: higher-magnification pictures of the retina. $Tmem98^{A193P/A193P}$, $Tmem98^{H196P/H196P}$, $Tmem98^{A193P/H196P}$, and $Tmem98^{I135T/H196P}$ retinas all have scattered white spots (*left*) and folds in the outer nuclear layer and sometimes the inner retinal layers as well (*center* and *right*). *Scale bars*: 1 mm (**B**, *center*), 100 µm (**B**, *right*).

Investigative Ophthalmology & Visual Science

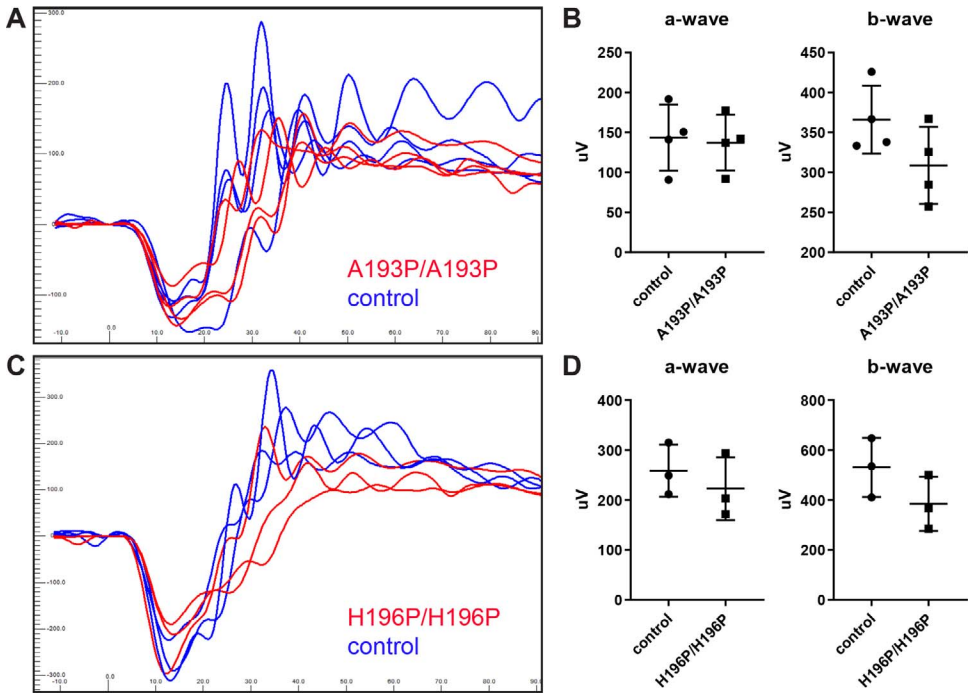

Figure 3. *Tmem98*$^{A193P/A193P}$ and *Tmem98*$^{H196P/H196P}$ mice have a normal ERG response. (**A**, **B**) Littermates, four *Tmem98*$^{A193P/A193P}$ mice and four control mice (two wild-type and two *Tmem98*$^{A193P/+}$) were tested at 4 months of age. (**A**) ERG traces of *Tmem98*$^{A193P/A193P}$ mice (*red lines*) and control mice (*blue lines*). Shown are the responses at 3 cd.s/m^2 (average of four flashes) for the left eye. (**B**) Comparison of a-wave amplitudes (*right*) and b-wave amplitudes (*left*), average of left and right eye for each mouse. There is no significant difference between *Tmem98*$^{A193P/A193P}$ and control mice (a-wave, unpaired *t*-test with Welch's correction, $P = 0.82$ and b-wave, unpaired *t*-test with Welch's correction, $P = 0.13$). (**C**, **D**) Three *Tmem98*$^{H196P/H196P}$ mice and three control mice (two wild-type and one *Tmem98*$^{H196P/+}$) were tested at 6 months of age. (**C**) ERG traces of *Tmem98*$^{H196P/H196P}$ mice (*red lines*) and control mice (*blue lines*). Shown are the responses at 3 cd.s/m^2 (average of four flashes) for the left eye. (**D**) Comparison of a-wave amplitudes (*left*) and b-wave amplitudes (*right*), average of left and right eye for each mouse. There is no significant difference between *Tmem98*$^{H196P/H196P}$ and control mice (a-wave, unpaired *t*-test with Welch's correction, $P = 0.49$ and b-wave, unpaired *t*-test with Welch's correction, $P = 0.19$).

Statistics

For the data shown in Figures 1, 2, and 3 and Supplementary Figure S7 the graphs were created and unpaired *t*-tests with Welch's correction were performed using the program Graphpad Prism (GraphPad Software, San Diego, CA, USA). For the data shown in Table 2 and Supplementary Tables S3 and S4, χ^2 tests were performed using http://graphpad.com/quickcalcs (in the public domain). A value of $P < 0.05$ was considered significant.

Results

Rwhs Is a Missense Mutation of the *Tmem98* Gene

The *N*-ethyl-*N*-nitrosourea (ENU)-induced mouse mutation retinal white spots (*Rwhs*) was found in a screen for dominant eye mutations.[37] Mice heterozygous for the mutation have white patches on retinal imaging, apparently corresponding to folds or invaginations of the photoreceptor layers (Figs. 1A, 1B). Initial mapping indicated that *Rwhs* was located within an 8.5-Mb region of chromosome 11.[37] The retinal phenotype was found on a mixed Balb/c and C3H background. When *Rwhs* mutant mice were backcrossed to the C57BL/6J strain to refine the genetic mapping, some obligate heterozygous mice had retinas with a normal appearance, indicating that the dominant *Rwhs* phenotype is not completely penetrant and that modifiers in the C57BL/6J strain can attenuate it (Supplementary Figs. S1A–D). Crossing *Rwhs* to the wild-derived *CAST* strain to introduce a different and diverse genetic background restored the retinal phenotype (Supplementary Figs. S1E, S1F). Intercrossing of heterozygous mice produced no homozygous offspring at weaning, whereas at late gestation (embryonic day [E]17.5–E18.5) fetuses of the three expected genotypes were present at Mendelian ratios indicating that homozygous *Rwhs* is perinatally lethal (Table 2) (an initial report suggesting that homozygous *Rwhs* mice were viable was incorrect and due to mapping errors[37]). We mapped this lethal phenotype by intercrossing recombinant animals and refined the critical interval to a 200-kb region between the single nucleotide polymorphism markers rs216663786 and rs28213460 on chromosome 11. This region contains the *Tmem98* gene and parts of the *Myo1d* and *Spaca3* genes. We amplified and sequenced all the exons and flanking regions from this region from *Rwhs* mutant mice along with controls. In addition we captured and sequenced all genomic DNA in the candidate interval. We found only a single nucleotide change in the mutant strain compared to the strain of origin, a T to C transition, in exon 5 of *Tmem98* (position 11:80,817,609 Mouse Dec. 2011 (GRCm38/mm10) Assembly [https://genome.ucsc.edu/, in the public domain]) (Fig. 1C). This mutation leads to the substitution of the nonpolar aliphatic amino acid, isoleucine, by the polar amino acid threonine (I135T, numbering from entry Q91X86, http://www.uniprot.org, in the public domain). This amino acid substitution is predicted to be possibly damaging by the polymorphism prediction tool PolyPhen-2.[42]

TMEM98 is a 226-amino acid protein annotated with a transmembrane domain spanning amino acids 4 to 24 close to the N-terminus (http://www.uniprot.org, in the public do-

Table 2. *Tmem98*$^{Rwbs/+}$ Intercross Genotyping Results

Age	WT	*Rwbs*/+	*Rwbs/Rwbs*	Total	*P**
Adult	34	79	0	113	<0.0001
E17.5–E18.5	2	12	5	19	0.3225

WT, wild type.
* Test for significance using χ^2 test.

main). It is highly conserved across species; mouse and human TMEM98 share 98.7% amino acid identity, and between mouse and *Ciona intestinalis*, the closest invertebrate species to the vertebrates, there is 38.6% amino acid identity in which I135 is conserved (Supplementary Fig. S2). TMEM98 has been reported to be a single-pass type II transmembrane protein in which the C-terminal part is extracellular.[49] *TMEM98* is widely expressed and is reported to be most highly expressed in human and mouse RPE (http://www.biogps.org, in the public domain). We confirmed its high expression in the RPE and, within the retina, we also find expression at a lower level in the ganglion cell layer (Fig. 1D). To assess retinal function, electroretinography was carried out on *Tmem98*$^{I135T/+}$ and wild-type mice (Figs. 1E, 1F). There were no significant differences in the a-wave or b-wave amplitudes between the *Tmem98*$^{I135T/+}$ and wild-type mice.

We also investigated the effect of loss of function of *Tmem98*. Heterozygous loss-of-function mice are viable and fertile and have normal retinas (Supplementary Figs. S6D, S6F). Matings of heterozygous mice carrying the "knockout first" *Tmem98*^{tm1a} allele produced no homozygous offspring (Supplementary Table S3), demonstrating that loss of function of *Tmem98* is lethal. At E16.5 to E17.5 the three expected genotypes were present at Mendelian ratios (Supplementary Table S3), and in one litter collected at birth there were three homozygotes and three wild types indicating that lethality occurs between birth and weaning.

The Human Nanophthalmos Missense Mutations Cause a Retinal Phenotype in the Mouse

Three mutations in *TMEM98* have been implicated in autosomal dominant nanophthalmos in human families.[12,13] Two are missense mutations, A193P and H196P. Both missense mutations affect amino acids that are highly conserved (Supplementary Fig. S2). Both are predicted to be probably damaging by the polymorphism prediction tool PolyPhen-2.[42]

To investigate the effect of the two missense mutations we used CRISPR-Cas9 to introduce A193P and H196P into the mouse gene and established lines carrying each. Western blot analysis using a validated anti-TMEM98 antibody (Supplementary Fig. S3A) showed that the mutant proteins are expressed (Supplementary Fig. S3B). Heterozygous mice for both missense mutations were viable and fertile and did not exhibit any gross eye or retinal defects when examined between 5 and 9 months of age (Supplementary Fig. S4, *Tmem98*$^{A193P/+}$, $n = 10$; *Tmem98*$^{H196P/+}$, $n = 19$). In contrast to the *Tmem98*^{I135T} and knockout alleles, homozygotes for both the *Tmem98*^{A193P} and *Tmem98*^{H196P} alleles were viable and found at the expected Mendelian ratios (Supplementary Table S4). The eyes of homozygous mice do not appear to be significantly different in axial length when compared to wild-type eyes (Fig. 2A). Although the mean length of homozygous *Tmem98*^{H196P} eyes is ~7% smaller than in controls, this does not have statistical support ($P = 0.1$). From approximately 3 months of age we found that white patches developed on the retinas of the homozygous mice and on histologic examination we found folds or invaginations in the retinal layers (Fig. 2B). The appearance of the white patches was progressive; at younger ages the retinas of some homozygous mice appeared normal, with patches becoming apparent as they aged (Supplementary Fig. S5). In the A193P line only six of seven homozygotes were found to have retinal defects at 6 months of age; the seventh developed white patches on the retina by 9 months. In the H196P line 4/20 homozygous mice that were examined between 3 and 3.5 months of age appeared to have normal retinas. We crossed the lines together to generate compound heterozygotes. All *Tmem98*$^{A193P/H196P}$ ($n = 4$), *Tmem98*$^{I135T/A193P}$ ($n = 7$), and *Tmem98*$^{I135T/H196P}$ ($n = 5$) mice examined also displayed a similar phenotype of white patches on the retina (Fig. 2B and data not shown). We also crossed *Tmem98*^{H196P} mice with mice carrying a loss-of-function allele *Tmem98*^{tm1b}. Compound heterozygous mice were viable, and of 17 mice examined, all had normal retinas except for one mouse that had three faint spots on one retina at 1 year of age (Supplementary Fig. S6). These results suggest that a threshold level of the mutant missense TMEM98^{H196P} and TMEM98^{A193P} proteins is required to elicit the formation of white patches on the retina and that the missense

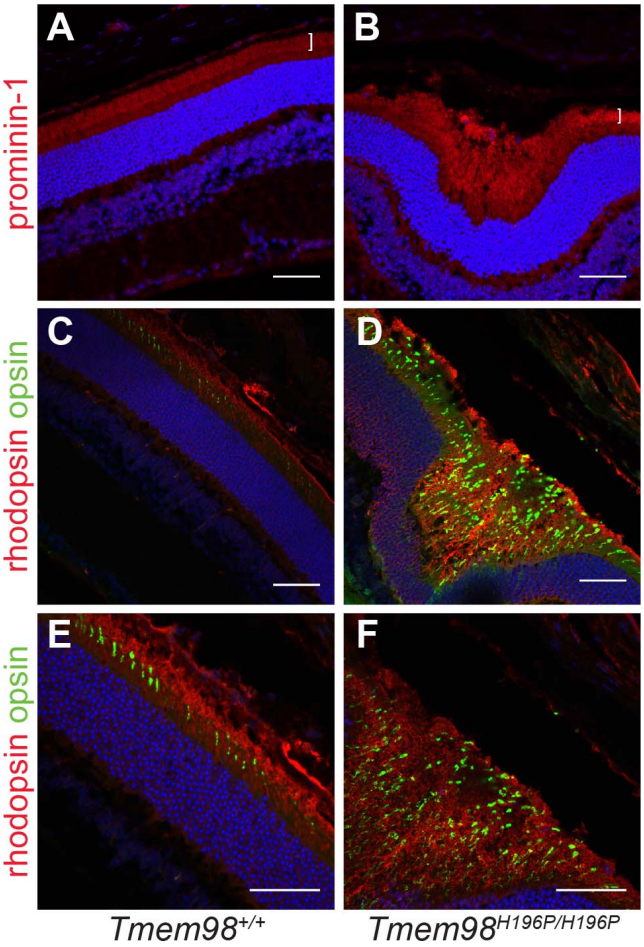

Figure 4. The interiors of the retinal folds found in the *Tmem98*$^{H196P/H196P}$ mutant mice are filled with excess outer segments. Immunostaining of retinal sections from wild-type mice (**A**, **C**, **E**) and *Tmem98*$^{H196P/H196P}$ mice (**B**, **D**, **F**). (**A**, **B**) Prominin-1 staining (*red*) shows that the outer segment layer (*white bracket*) is expanded in the retinal fold of the mutant (**B**) compared to wild type (**A**). (**C**–**F**) Rhodopsin (*red*) and opsin (*green*) staining shows that the interior of the retinal fold is filled with outer segments. DAPI staining is shown in *blue*. *Scale bars*: 50 μm.

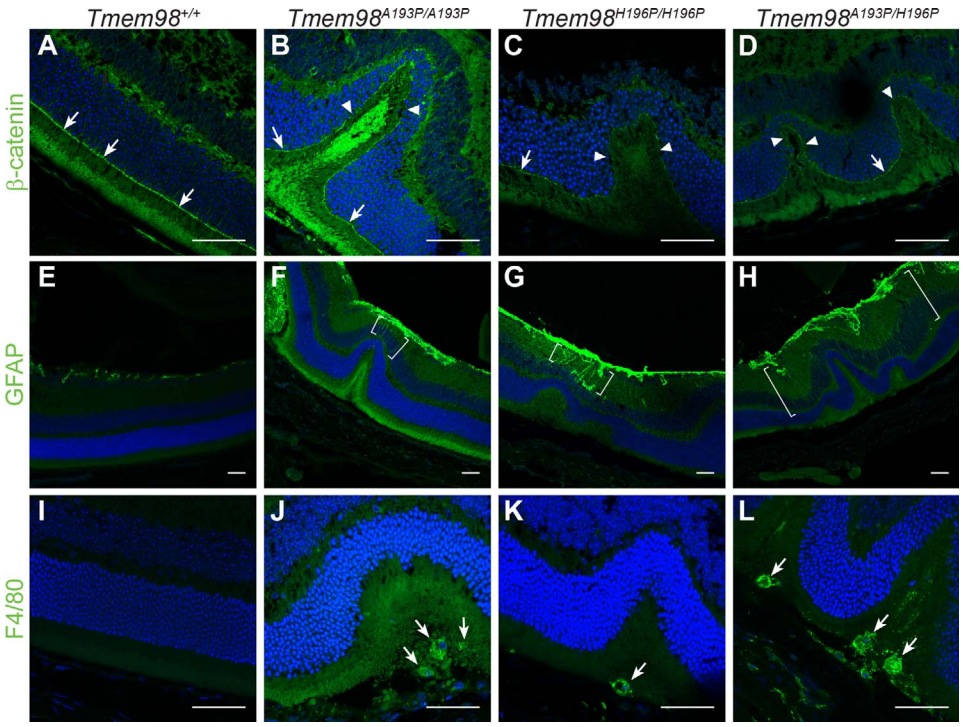

Figure 5. Characterization of the retinal folds in the *Tmem98* mutant mice. Immunostaining of retinal sections from wild-type mice (**A**, **E**, **I**), *Tmem98*$^{A193P/A193P}$ mice (**B**, **F**, **J**), *Tmem98*$^{H196P/H196P}$ mice (**C**, **G**, **K**), *Tmem98*$^{A193P/H196P}$ mice (**D**, **H**, **L**). (**A–D**) β-catenin staining (*green*) shows that the OLM is intact in the wild-type retina and in the areas either side of folds in the mutant retinas (*white arrows*), but in the folds of the mutant retinas the OLM is interrupted (*white arrowheads*). (**E–H**) GFAP staining (*green*) is normal in the wild-type retina, but above the folds in the mutant retinas there is abnormal GFAP staining extending toward the outer nuclear layer (areas between the *white brackets*). This indicates that in the mutants the retina is stressed in the folded regions and that retinal stress is confined to the folds. (**I–L**) F4/80 staining (*green*) reveals that macrophages have infiltrated into the areas below the folded outer nuclear layer containing excess photoreceptors in the mutant retinas (*white arrows*). Staining was not observed outside the folds in the mutant retinas. DAPI staining is shown in *blue*. *Scale bars*: 50 µm.

mutations found in the human nanophthalmos patients are not loss of function. Furthermore, mice heterozygous for *Tmem98*^{tm1b} with a wild-type allele do not have the retinal phenotype (Supplementary Fig. S6).

To assess retinal function, electroretinography was carried out on *Tmem98*$^{A193P/A193P}$, *Tmem98*$^{H196P/H196P}$, and control mice (Fig. 3). There were no significant differences in the a-wave or b-wave amplitudes between the control and the mutant mice. To determine if there was any deterioration in the retinal function of older mice we also tested *Tmem98*$^{H196P/H196P}$ and control mice at 9 to 11 months of age, but again we did not find any significant differences in the a-wave or b-wave amplitudes between the control and the mutant mice (Supplementary Fig. S7).

Characterization of the Retinal Folds Caused by the A193P and H196P Mutations

We investigated the retinal folds by immunostaining of retinal sections. We found that in the interior of retinal folds the outer segment layer is massively expanded as demonstrated by positive staining for the transmembrane protein prominin-1 and the rod and cone opsins (rhodopsin and ML opsin), indicating that the folds are filled with excess, disorganized outer segments or remnants of outer segments (Fig. 4).

The retinal folds seen in other mutant mouse lines are accompanied by defects in the OLM. This structure is formed by adherens junctions between the Müller glia cells and the photoreceptors. We investigated the integrity of the OLM in our mutant mice by staining for β-catenin (Figs. 5A–D). In control mice and in the regions of the retinas of mutant mice unaffected by folds the OLM appeared intact. However, at the folds the OLM is clearly disrupted and gaps can be seen suggesting that cell–cell connections have been broken. Reactive gliosis indicated by upregulation of glial fibrillary acidic protein (GFAP) in the Müller cells is a response to retinal stress, injury, or damage.[50] We observed abnormal GFAP staining in the mutant retinas that was confined to the regions with folds, indicating that in these areas, but not elsewhere in the retina, there is a stress response (Figs. 5F–5H; Supplementary Figs. S8A–D). We also stained for F4/80, a marker for macrophages/microglia. In the mutant retinas positive staining was found in the interior of retinal folds but not elsewhere in the photoreceptor layer (Figs. 5J–L; Supplementary Figs. S8F, S8H). The amoeboid shape of the positively stained cells suggests that they are macrophages that have infiltrated into the retinal folds containing excess and disorganized outer segments and that they are phagocytosing degenerating outer segments. We did not observe melanin within the macrophages indicating that they had not engulfed pigmented RPE cells. Finally, we examined by transmission electron microscopy the ultrastructural architecture of the boundary between the RPE and outer segments (Fig. 6). For the homozygous mutants, in retinal areas without folds, the boundary between outer segments and RPE appeared normal (compare Fig. 6A with Figs. 6B and 6D). However, in the areas with folds the outer segments were disorganized and appeared to be degenerating, with cavities and other cellular debris apparent (Figs. 6C, 6E).

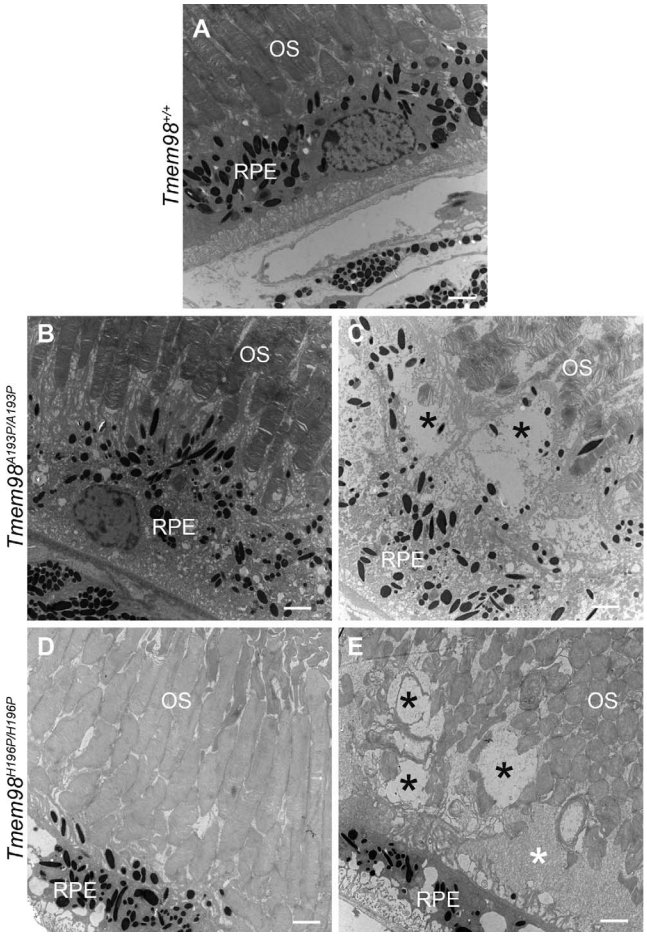

FIGURE 6. Ultrastructural analysis of the RPE and outer segment boundary. (**A**) Wild-type mice are normal. (**B**, **D**) In mutant mice from retinal regions with no folds the outer segments adjacent to the RPE appear normal. (**C**, **E**) In retinal areas with folds the outer segments abutting the RPE appear abnormal and disorganized. Several large vacuoles (indicated by *black asterisks*) can be seen. In (**E**) there is an area containing cellular debris (indicated by a *white asterisk*). *Tmem98*$^{A193P/A193P}$ (**B**, **C**) and *Tmem98*$^{H196P/H196P}$ (**D**, **E**). OS, outer segments. *Scale bars*: 2 µm.

DISCUSSION

Rwhs Is Caused by a Missense Mutation in *Tmem98* That Is Homozygous Lethal

Here we report that the ENU-induced dominant retinal white spotting phenotype, *Rwhs*, is caused by an I135T missense mutation in the highly conserved transmembrane protein encoding gene *Tmem98*. We also found that when homozygous the *Tmem98*^{I135T} allele is perinatally lethal. *Tmem98* was one of the genes included in an international project to produce and phenotype knockout mouse lines for 20,000 genes.[51] The targeted allele, *Tmem98*^{tm1a}, was subjected to a high-content phenotyping pipeline (results available at http://www.mousephenotype.org/data/genes/MGI:1923457, in the public domain). It was found to be lethal preweaning as homozygotes, but no significant heterozygous phenotypic variation from wild type was reported. Neither the slit-lamp analysis nor our retinal examination found any eye defects in knockout heterozygous mice (Supplementary Figs. S6D, S6F). We also found that *Tmem98*^{tm1a} is homozygous lethal and narrowed the stage of lethality to the perinatal stage (Supplementary Table S3). This suggests that haploinsufficency for TMEM98 protein does not cause a retinal phenotype and that the I135T mutation in TMEM98 is not a loss-of-function allele but changes the protein's function leading to the retinal white spotting phenotype.

Phenotype of Human Nanophthalmos-Associated *TMEM98* Missense Mutations in the Mouse

Tmem98 has been previously suggested to be a novel chemoresistance-conferring gene in hepatoceullular carcinoma.[52] It has also been reported to be able to promote the differentiation of T helper 1 cells and to be involved in the invasion and migration of lung cancer cells.[49,53] Recently it has been reported that TMEM98 interacts with MYRF and prevents its autocatalytic cleavage.[54] In relation to human disease, two *TMEM98* missense mutations, A193P and H196P, have been reported to be associated with dominant nanophthalmos.[12,13] We introduced these mutations into the mouse gene and found that mice homozygous for either, or compound heterozygous for both, developed white patches on their retinas accompanied by retinal folds, replicating the dominant phenotype found in the ENU-induced allele. We also observed for all three alleles separation of the RPE away from the neural retina in the areas under the folds. Homozygous mice for the knockout allele do not survive after birth (Supplementary Table S3). In contrast, the two human-equivalent mutations in the mouse are homozygous viable (Supplementary Table S4), and the mouse mutation I135T, when in combination with a knockout allele, is also viable (data not shown). Furthermore, the H196P missense mutation in combination with a gene knockout has no detectable eye phenotype and the mice are viable (Supplementary Fig. S6). This suggests that the three missense mutations described here are probably not null. It is also unlikely that the two human-equivalent recessive mutations are partial loss of function as when in combination with the knockout allele they show no phenotype, rather than a more severe phenotype that would be expected for a hypomorphic allele. Likewise, these data suggest that they are not dominant negative alleles as these would be expected to exhibit a more severe phenotype when in combination with a null allele. We think it is most likely that they are gain of function with, in the case of H196P at least, a threshold dosage requirement. However, the phenotypes are different from the reported dominant nanophthalmos caused by the same mutations in humans, so the nature of the effect of the missense mutations on protein function will be the subject of future work.

Other genes causing nanophthalmos may also be gain of function. The serine protease *PRSS56* is a recessive posterior microphthalmia or nanophthalmos mutant gene in humans, with both identified mutations affecting the C-terminus of the protein.[8] The mouse mutant model of this gene, which produces a variable and slight reduction in ocular length, is a splice site mutation resulting in a truncated protein that nevertheless has normal protease activity in vitro.[8] Recently the phenotype of a null allele of *Prss56* has been described, and it does cause some reduction in ocular size and hyperopia.[36]

The mouse model of the nanophthalmos gene, *Mfrp*, does not reproduce the human phenotype. Rather, loss of function of this gene results in white spots apparent on retinal imaging (retinitis punctata albicans), but these have a different origin from the phenotype we observe, and progress to photoreceptor degeneration. It has been reported that the *Mfrp* knockout mice have eyes that are slightly (but not statistically significantly) smaller, by approximately 2% in axial length.[35] Our analysis of the human-equivalent mouse *Tmem98* mutations shows that that neither has statistically significant

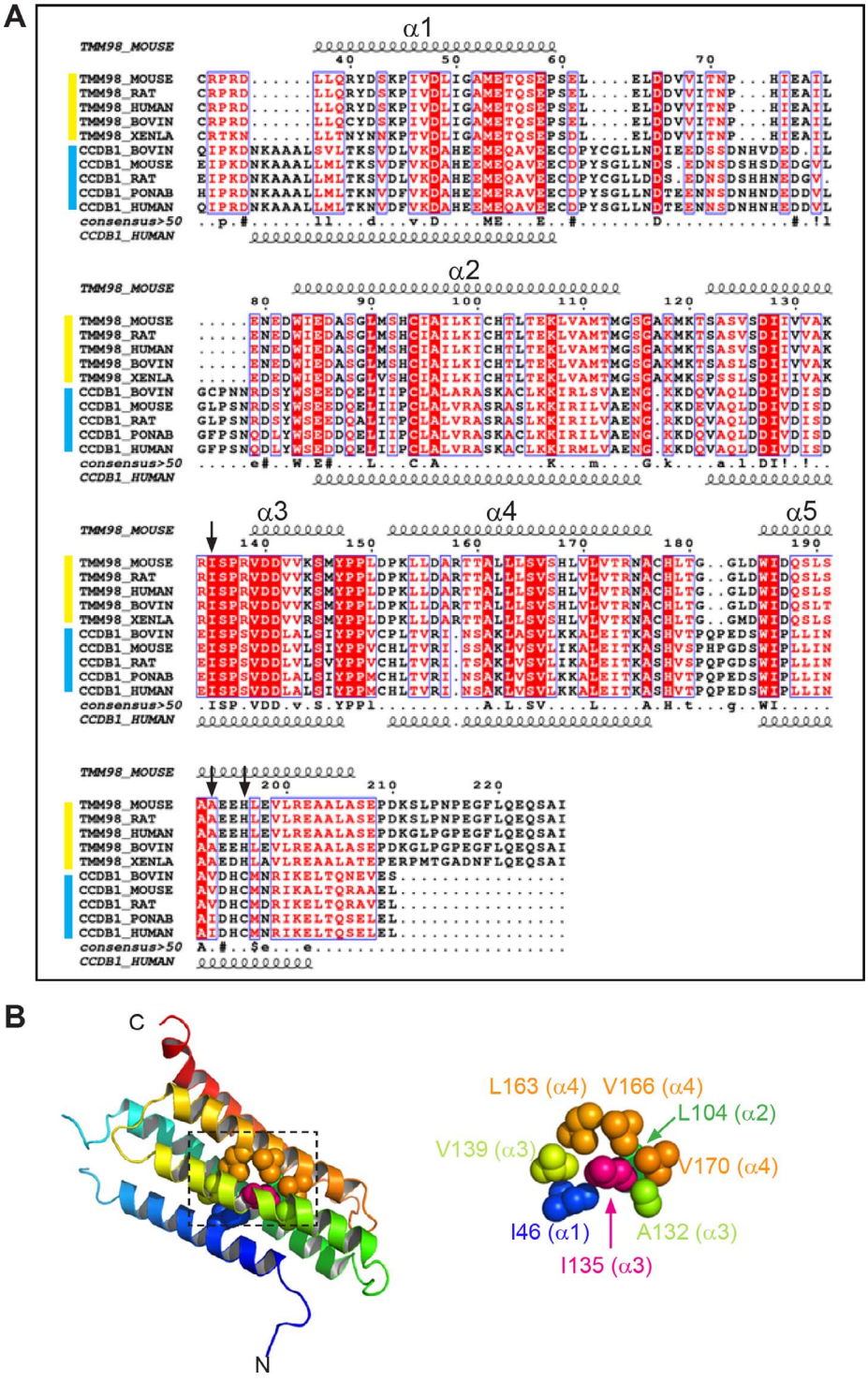

Figure 7. TMEM98 protein structure and predicted effect of the I135T mutation. (**A**) Alignment of TMEM98 proteins (*yellow group*) and CCNDBP1 proteins (*blue group*). The positions of predicted α-helices (1–5) are indicated by the *curly lines*. The positions of the three missense mutations are indicated by the *black arrows*. (**B**) Helical bundle based upon the crystal structure of CCNDBP1 (c3ay5A). The N- and C-terminal ends are indicated. The region surrounding I135 (*dashed box*) is enlarged on the *right* showing the hydrophobic interactions within 5 Å of I135.

size reductions, although the H196P line is ~7% shorter. It is worth noting that different strains of mice have measurably different ocular size. Strain differences of up to 2% and sex differences of over 1.5% have been reported.[48]

Two genes that are infrequently associated with nanophthalmos, *CRB1* and *BEST1*, can both produce a mouse phenotype apparently indistinguishable from the one we describe here. Furthermore, the knockout mouse model of the nuclear receptor gene, *Nrl*, also develops retinal folds during postnatal life.[55] The *Nrl* mutant eye has defects in the OLM, a component of which is the CRB1 protein. The *Tmem98* mutations have OLM defects, but we cannot ascertain whether these defects are the primary cause of the folds or a secondary consequence.

Retinal folds are a characteristic of nanophthalmic eyes, and this is usually attributed to a differential growth of neural retina within the smaller optic cup. Our data show that folds can be seen in a normal-sized eye, but we do not know whether there is nevertheless excess growth of the neural retina. The retinal defects we see are not associated with an ERG deficit, suggesting that the rest of the retina, unaffected by the folds, is functionally normal.

Notable is the detachment of the retina from the RPE within the folds. In the *Nrl* and *Crb1* mutant eyes the photoreceptors that have lost their connection to the RPE can be seen to degenerate. We see no evidence of photoreceptor degeneration in the *Tmem98* mutants. The mechanism of the pathology is still unclear. As *Tmem98* is strongly expressed in the RPE, and not at all in the photoreceptors, it is likely that RPE is the affected tissue. The key observation in these and other mouse models of nanophthalmos is that the defects are focal and progressive, suggesting that secondary events exacerbate an underlying but (given ERG data) nonpathological defect. The accumulation of photoreceptor cell debris below the retinal folds suggests a focal defect in outer segment phagocytosis but one that does not lead to photoreceptor degeneration. Three of the genes associated with nanophthalmos are expressed in the RPE: *Tmem98*, *Best1*, and *Mfrp. Crb1* is expressed in photoreceptors and *Prss56*, a secreted serine protease, is expressed in the Müller cells. It is possible that these genes interact and affect a common pathway; indeed upregulation of *Prss56* has been observed in *Mfrp* mutants.[56]

Effect on TMEM98 Protein Structure of the Missense Mutations

TMEM98 has structural homology to cyclin-D1–binding protein 1 (CCNDBP1) and contains a Grap2 and cyclin-D–interacting (GCIP) domain (pfam13324) spanning amino acids 49 to 152. Based upon the crystal structure of CCNDBP1, following the N-terminal transmembrane domain, TMEM98 is predicted to have a five-helix bundle structure using PHYRE2[44] (Fig. 7A). I135 is located in the third α-helix completely buried within a sterically close-packed hydrophobic core of the domain where it has hydrophobic interactions with amino acids from four of the α-helices (Fig. 7B). SCWRL[46] and FoldX[47] stability calculations indicate that the *Rwbs* mutation T135 is only very mildly destabilizing in this homology model. Its side chain does not show steric clashes with other neighboring atoms and its buried hydroxyl group forms a favorable hydrogen bond with the main-chain oxygen atom of A132. The stability energy calculation on the mutant TMEM98 domain structure (mean $\Delta\Delta G$) is 0.28 kcal/mol (>1.6 kcal/mol is considered destabilizing). The genetic evidence shows that I135T is not loss of function. The detrimental effect of a mutation leading to loss of thermodynamic stability can be compensated for by the creation of novel functions.[57] This might be the case with the I135T mutation. The two missense mutations that are associated with nanophthalmos in humans both introduce a proline in the middle of the final α-helix of the protein, which would likely lead to disruption of the secondary structure of the protein.[58] The recent finding that TMEM98 binds to and prevents the self-cleavage of the oligodendrocyte transcription factor MYRF[54] (also highly expressed in the RPE, http://www.biogps.org, in the public domain) will perhaps lead to a mechanistic explanation, although the part of TMEM98 that binds to MYRF was mapped to the N-terminal 88 amino acids, and a region between 55 and 152 amino acids was shown to be required for the cleavage inhibition. As the nanophthalmos patient-specific missense mutations are more C-terminal, their effect on this reported interaction will be the subject of future work.

Acknowledgments

The authors thank Morag Robertson for help with genotyping, Craig Nicol and Connor Warnock for help with photography, the IGMM Advanced Imaging Resource for help with imaging, Edinburgh University Bioresearch and Veterinary Services for animal husbandry, and MRC Human Genetics Unit scientific support services.

Supported by the MRC University Unit award to the MRC Human Genetics Unit.

Disclosure: **S.H. Cross**, None; **L. Mckie**, None; **M. Keighren**, None; **K. West**, None; **C. Thaung**, None; **T. Davey**, None; **D.C. Soares**, None; **L. Sanchez-Pulido**, None; **I.J. Jackson**, None

References

1. Verma AS, FitzPatrick DR. Anophthalmia and microphthalmia. *Orphanet J Rare Dis*. 2007;2:47.
2. Carricondo PC, Andrade T, Prasov L, Ayres BM, Moroi SE. Nanophthalmos: a review of the clinical spectrum and genetics. *J Ophthalmol*. 2018;2018:2735465.
3. Sundin OH, Leppert GS, Silva ED, et al. Extreme hyperopia is the result of null mutations in MFRP, which encodes a Frizzled-related protein. *Proc Natl Acad Sci U S A*. 2005;102:9553–9558.
4. Ayala-Ramirez R, Graue-Wiechers F, Robredo V, Amato-Almanza M, Horta-Diez I, Zenteno JC. A new autosomal recessive syndrome consisting of posterior microphthalmos, retinitis pigmentosa, foveoschisis, and optic disc drusen is caused by a MFRP gene mutation. *Mol Vis*. 2006;12:1483–1489.
5. Zenteno JC, Buentello-Volante B, Quiroz-González MA, Quiroz-Reyes MA. Compound heterozygosity for a novel and a recurrent MFRP gene mutation in a family with the nanophthalmos-retinitis pigmentosa complex. *Mol Vis*. 2009;15:1794–1798.
6. Neri A, Leaci R, Zenteno JC, Casubolo C, Delfini E, Macaluso C. Membrane frizzled-related protein gene–related ophthalmological syndrome: 30-month follow-up of a sporadic case and review of genotype-phenotype correlation in the literature. *Mol Vis*. 2012;18:2623–2632.
7. Gal A, Rau I, El Matri L, et al. Autosomal-recessive posterior microphthalmos is caused by mutations in PRSS56, a gene encoding a trypsin-like serine protease. *Am J Hum Genet*. 2011;88:382–390.
8. Nair KS, Hmani-Aifa M, Ali Z, et al. Alteration of the serine protease PRSS56 causes angle-closure glaucoma in mice and posterior microphthalmia in humans and mice. *Nat Genet*. 2011;43:579–584.
9. Orr A, Dubé M-P, Zenteno JC, et al. Mutations in a novel serine protease PRSS56 in families with nanophthalmos. *Mol Vis*. 2011;17:1850–1861.
10. Kiefer AK, Tung JY, Do CB, et al. Genome-wide analysis points to roles for extracellular matrix remodeling, the visual cycle, and neuronal development in myopia. *PLoS Genet*. 2013;9:e1003299.
11. Verhoeven VJ, Hysi PG, Wojciechowski R, et al. Genome-wide meta-analyses of multiancestry cohorts identify multiple new susceptibility loci for refractive error and myopia. *Nat Genet*. 2013;45:314–318.
12. Awadalla MS, Burdon KP, Souzeau E, et al. Mutation in TMEM98 in a large white kindred with autosomal dominant nanophthalmos linked to 17p12-q12. *JAMA Ophthalmol*. 2014;132:970–977.
13. Khorram D, Choi M, Roos BR, et al. Novel TMEM98 mutations in pedigrees with autosomal dominant nanophthalmos. *Mol Vis*. 2015;21:1017–1023.

14. Sun W, Zhang Q. Does the association between TMEM98 and nanophthalmos require further confirmation? *JAMA Ophthalmol*. 2015;133:358–359.
15. Boon CJ, Klevering BJ, Leroy BP, Hoyng CB, Keunen JE, den Hollander AI. The spectrum of ocular phenotypes caused by mutations in the BEST1 gene. *Prog Retin Eye Res*. 2009;28:187–205.
16. Marmorstein AD, Marmorstein LY, Rayborn M, Wang X, Hollyfield JG, Petrukhin K. Bestrophin, the product of the Best vitelliform macular dystrophy gene (VMD2), localizes to the basolateral plasma membrane of the retinal pigment epithelium. *Proc Natl Acad Sci U S A*. 2000;97:12758–12763.
17. Petrukhin K, Koisti MJ, Bakall B, et al. Identification of the gene responsible for Best macular dystrophy. *Nat Genet*. 1998;19:241–247.
18. Yardley J, Leroy BP, Hart-Holden N, et al. Mutations of VMD2 splicing regulators cause nanophthalmos and autosomal dominant vitreoretinochoroidopathy (ADVIRC). *Invest Ophthalmol Vis Sci*. 2004;45:3683–3689.
19. Burgess R, Millar ID, Leroy BP, et al. Biallelic mutation of BEST1 causes a distinct retinopathy in humans. *Am J Hum Genet*. 2008;82:19–31.
20. Pellikka M, Tanentzapf G, Pinto M, et al. Crumbs, the Drosophila homologue of human CRB1/RP12, is essential for photoreceptor morphogenesis. *Nature*. 2002;416:143–149.
21. den Hollander AI, Jacoline B, de Kok YJ, et al. Mutations in a human homologue of Drosophila crumbs cause retinitis pigmentosa (RP12). *Nat Genet*. 1999;23:217–221.
22. den Hollander AI, Heckenlively JR, van den Born LI, et al. Leber congenital amaurosis and retinitis pigmentosa with Coats-like exudative vasculopathy are associated with mutations in the crumbs homologue 1 (CRB1) gene. *Am J Hum Genet*. 2001;69:198–203.
23. Henderson RH, Mackay DS, Li Z, et al. Phenotypic variability in patients with retinal dystrophies due to mutations in CRB1. *Br J Ophthalmol*. 2011;95:811–817.
24. Zenteno JC, Buentello-Volante B, Ayala-Ramirez R, Villanueva-Mendoza C. Homozygosity mapping identifies the Crumbs homologue 1 (Crb1) gene as responsible for a recessive syndrome of retinitis pigmentosa and nanophthalmos. *Am J Med Genet A*. 2011;155:1001–1006.
25. Paun CC, Pijl BJ, Siemiatkowska AM, et al. A novel crumbs homolog 1 mutation in a family with retinitis pigmentosa, nanophthalmos, and optic disc drusen. *Mol Vis*. 2012;18:2447–2453.
26. Marmorstein LY, Wu J, McLaughlin P, et al. The light peak of the electroretinogram is dependent on voltage-gated calcium channels and antagonized by bestrophin (best-1). *J Gen Physiol*. 2006;127:577–589.
27. Milenkovic A, Brandl C, Milenkovic VM, et al. Bestrophin 1 is indispensable for volume regulation in human retinal pigment epithelium cells. *Proc Natl Acad Sci U S A*. 2015;112:E2630–E2639.
28. Zhang Y, Stanton JB, Wu J, et al. Suppression of Ca2+ signaling in a mouse model of Best disease. *Hum Mol Genet*. 2010;19:1108–1118.
29. Mehalow AK, Kameya S, Smith RS, et al. CRB1 is essential for external limiting membrane integrity and photoreceptor morphogenesis in the mammalian retina. *Hum Mol Genet*. 2003;12:2179–2189.
30. van de Pavert SA, Kantardzhieva A, Malysheva A, et al. Crumbs homologue 1 is required for maintenance of photoreceptor cell polarization and adhesion during light exposure. *J Cell Sci*. 2004;117:4169–4177.
31. van de Pavert SA, Meuleman J, Malysheva A, et al. A single amino acid substitution (Cys249Trp) in Crb1 causes retinal degeneration and deregulates expression of pituitary tumor transforming gene Pttg1. *J Neurosci*. 2007;27:564–573.
32. Kameya S, Hawes NL, Chang B, Heckenlively JR, Naggert JK, Nishina PM. Mfrp, a gene encoding a frizzled related protein, is mutated in the mouse retinal degeneration 6. *Hum Mol Genet*. 2002;11:1879–1886.
33. Fogerty J, Besharse JC. 174delG mutation in mouse MFRP causes photoreceptor degeneration and RPE atrophy. *Invest Ophthalmol Vis Sci*. 2011;52:7256–7266.
34. Hawes NL, Chang B, Hageman GS, et al. Retinal degeneration 6 (rd6): a new mouse model for human retinitis punctata albescens. *Invest Ophthalmol Vis Sci*. 2000;41:3149–3157.
35. Velez G, Tsang SH, Tsai Y-T, et al. Gene therapy restores Mfrp and corrects axial eye length. *Sci Rep*. 2017;7:16151.
36. Paylakhi S, Labelle-Dumais C, Tolman NG, et al. Muller glia-derived PRSS56 is required to sustain ocular axial growth and prevent refractive error. *PLoS Genet*. 2018;14:e1007244.
37. Thaung C, West K, Clark BJ, et al. Novel ENU-induced eye mutations in the mouse: models for human eye disease. *Hum Mol Genet*. 2002;11:755–767.
38. White JK, Gerdin A-K, Karp NA, et al. Genome-wide generation and systematic phenotyping of knockout mice reveals new roles for many genes. *Cell*. 2013;154:452–464.
39. Skarnes WC, Rosen B, West AP, et al. A conditional knockout resource for the genome-wide study of mouse gene function. *Nature*. 2011;474:337–342.
40. Cong L, Ran FA, Cox D, et al. Multiplex genome engineering using CRISPR/Cas systems. *Science*. 2013;339:819–823.
41. Sievers F, Wilm A, Dineen D, et al. Fast, scalable generation of high-quality protein multiple sequence alignments using Clustal Omega. *Mol Syst Biol*. 2011;7:539.
42. Adzhubei IA, Schmidt S, Peshkin L, et al. A method and server for predicting damaging missense mutations. *Nat Methods*. 2010;7:248–249.
43. Soding J. Protein homology detection by HMM-HMM comparison. *Bioinformatics*. 2005;21:951–960.
44. Kelley LA, Mezulis S, Yates CM, Wass MN, Sternberg MJ. The Phyre2 web portal for protein modeling, prediction and analysis. *Nat Protoc*. 2015;10:845–858.
45. Janson G, Zhang C, Prado MG, Paiardini A. PyMod 2.0: improvements in protein sequence-structure analysis and homology modeling within PyMOL. *Bioinformatics*. 2017;33:444–446.
46. Wang Q, Canutescu AA, Dunbrack RL Jr. SCWRL and MolIDE: computer programs for side-chain conformation prediction and homology modeling. *Nat Protoc*. 2008;3:1832–1847.
47. Schymkowitz J, Borg J, Stricher F, Nys R, Rousseau F, Serrano L. The FoldX web server: an online force field. *Nucleic Acids Res*. 2005;33:W382–W388.
48. Puk O, Dalke C, Favor J, de Angelis MH, Graw J. Variations of eye size parameters among different strains of mice. *Mamm Genome*. 2006;17:851–857.
49. Fu W, Cheng Y, Zhang Y, et al. The secreted form of transmembrane protein 98 promotes the differentiation of T helper 1 cells. *J Interferon Cytokine Res*. 2015;35:720–733.
50. Lewis GP, Fisher SK. Up-regulation of glial fibrillary acidic protein in response to retinal injury: its potential role in glial remodeling and a comparison to vimentin expression. *Int Rev Cytol*. 2003;230:264–290.
51. Brown SD, Holmes CC, Mallon A-M, Meehan TF, Smedley D, Wells S. High-throughput mouse phenomics for characterizing mammalian gene function. *Nat Rev Genet*. 2018;19:357–370.
52. Ng KT, Lo CM, Guo DY, et al. Identification of transmembrane protein 98 as a novel chemoresistance-conferring gene in hepatocellular carcinoma. *Mol Cancer Ther*. 2014;13:1285–1297.
53. Mao M, Chen J, Li X, Wu Z. siRNA-TMEM98 inhibits the invasion and migration of lung cancer cells. *Int J Clin Exp Pathol*. 2015;8:15661–15669.

Investigative Ophthalmology & Visual Science

54. Huang H, Teng P, Du J, et al. Interactive repression of MYRF self-cleavage and activity in oligodendrocyte differentiation by TMEM98 protein. *J Neurosci*. 2018;38:9829–2839.
55. Stuck MW, Conley SM, Naash MI. Defects in the outer limiting membrane are associated with rosette development in the Nrl-/- retina. *PLoS One*. 2012;7:e32484.
56. Soundararajan R, Won J, Stearns TM, et al. Gene profiling of postnatal Mfrprd6 mutant eyes reveals differential accumulation of Prss56, visual cycle and phototransduction mRNAs. *PLoS One*. 2014;9:e110299.
57. Tokuriki N, Stricher F, Serrano L, Tawfik DS. How protein stability and new functions trade off. *PLoS Comput Biol*. 2008;4:e1000002.
58. Barlow DJ, Thornton JM. Helix geometry in proteins. *J Mol Biol*. 1988;201:601–619.

Investigative Ophthalmology & Visual Science